Nanoparticles Inhibit DNA Replication by Binding to DNA: Modeling and Experimental Validation

Kungang Li,[†] Xiaonan Zhao,[‡] Brian K. Hammer,[‡] Songyan Du,[†] and Yongsheng Chen[†,*]

[†]School of Civil and Environmental Engineering, Georgia Institute of Technology, Atlanta, Georgia 30332, United States and [‡]School of Biology, Georgia Institute of Technology, Atlanta, Georgia 30332, United States

ABSTRACT Predictive models are beneficial tools for researchers to use in prioritizing nanoparticles (NPs) for toxicological tests, but experimental evaluation can be time-consuming and expensive, and thus, priority should be given to tests that identify the NPs most likely to be harmful. For characterization of NPs, the physical binding of NPs to DNA molecules is important to measure, as interference with DNA function may be one cause of toxicity. Here, we determined the interaction energy between 12 types of NPs and DNA based on the Derjaguin–Landau–Verwey–Overbeek (DLVO) model and then predicted the affinity of the NPs for DNA. Using the single-molecule imaging technique known as atomic force microscopy (AFM), we experimentally determined the binding affinity of those NPs for DNA. Theoretical predictions and experimental observations of the binding affinity agreed well. Furthermore, the effect of NPs on DNA replication *in vitro* was investigated with the polymerase chain reaction (PCR) technique. The results showed that NPs with a high affinity for DNA strongly inhibited DNA replication, whereas NPs with low affinity had no or minimal effects on DNA replication. The methodology here is expected to benefit the genotoxicological testing of NPs as well as the design of safe NPs.

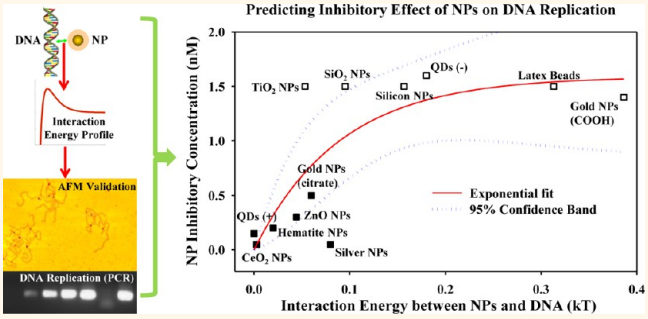

KEYWORDS: nanoparticle · DNA · model · genotoxicity · binding affinity · DLVO

Nanotechnology is a new frontier in science and technology in the 21st century that creates the potential for novel materials with unique functions and superior performances. However, concerns regarding the safety and health effects of engineered nanoparticles (NPs) arise alongside the booming nanotechnology industry. Numerous toxicological studies on NPs were published in the past decade, but many did not employ real nanosized materials, mainly because most NPs are subject to slow or fast aggregation in aqueous media.[1−6] The observed toxicity and related mechanisms in those studies are probably associated with the properties of aggregates/agglomerates.[7−10] At the interface between NPs and biological systems, some unaggregated NPs may have unique effects locally and exert different toxicity mechanisms compared with the aggregates; these mechanisms are not well documented yet. To explore the cytotoxic mechanisms of "real" NPs, we are developing systematic experimental approaches based on atomic force microscopy (AFM) to assess the effect of unaggregated NPs on single cells or biomolecules at the nanoscale.[11−13]

Primary or unaggregated NPs are likely to enter into biological cells[14−16] and subsequently exert toxic effects on intracellular structures like DNA.[17−19] Several mechanisms including oxidative stress and direct binding have been proposed to explain the genotoxicity of NPs.[19−23] Up to now, the mechanism of oxidative stress has been extensively studied on a wide range of NPs.[24−34] In contrast, the significance of direct binding of NPs to DNA is somewhat underestimated and has received less attention. Below we summarized a few studies related to the adverse effects induced by the binding activity of NPs to DNA. Our previous study showed that small quantum dots with a radius of 10 nm could permeate into bacterial cells and bind to DNA.[13] NP binding changed the normal conformation as well as the local electrical properties of

* Address correspondence to yongsheng.chen@ce.gatech.edu.

Received for review May 15, 2013 and accepted October 4, 2013.

Published online October 05, 2013
10.1021/nn402472k

DNA molecules.[11,13] A recent study also found that the binding of gold NPs causes structural changes including local denaturing and compaction to DNA.[35] Such changes may adversely interfere with the genetic functions of DNA, such as transcription, replication, and repair processes, that are crucial to maintain the normal metabolism of a living cell.[36−40] Specifically, NPs that bind to DNA with a high affinity could prohibit the normal functions of some critical DNA-binding proteins, such as RNA polymerase and DNA polymerase, by occupying protein-binding sites and impeding the movement of protein along the DNA, which could result in competitive inhibition of genetic functions.[38−41] It has been reported that functionalized gold NPs completely inhibited DNA transcription *in vitro* owing to the electrostatic interaction of NPs with DNA.[38−40] A computational simulation study also showed that C_{60} NPs strongly bind to DNA and might adversely impact the conformation and biological functions of DNA.[37] Furthermore, the binding of NPs to DNA might intervene in long-range charge transport through the DNA and thus interfere with signaling processes.[42] Thus, the interaction between NPs and DNA appears to play important roles in the toxicity of NPs and deserves a complete understanding of the underlying principle.

Because toxicological tests of NPs are time-consuming and expensive, scientists are developing models to predict the behavior and effects of NPs in biological systems,[43−45] which would allow researchers to streamline the toxicological testing of NPs by prioritizing NPs that are most likely to be harmful. Using theoretical models to describe the interaction between NPs and DNA is an important part of building an "ultimate" nanotoxicity-predicting model. Recently, several studies attempted to address the interaction of NPs with DNA using computational simulation techniques (mainly molecular dynamics simulations).[35,37,46] Although powerful, the application of these simulation techniques is restricted to ultrasmall NPs (<5 nm) and short DNA fragments due to the limitations of computational efficiency and capacity.[35,37,46] The complexity of these techniques also impedes their widespread use among researchers. Hence, it is necessary to develop some simpler techniques for investigating the NP−DNA interaction. It is well-known that in typical colloid physics the interfacial forces or energies fundamentally control the interaction between two objects. The Derjaguin−Landau−Verwey−Overbeek (DLVO) theory, for instance, is widely used to describe such interfacial interactions between charged objects in liquid.[47,48] According to the DLVO theory, the total interaction is comprised of van der Waals (vdW) and electrical double-layer (EDL) interactions. The interaction between spherical NPs and DNA can be described with the DLVO theory by treating the NP as a sphere and DNA as a uniformly charged cylinder[49−51] because the dimension of the DNA is significantly larger than the separation distance between its neighboring charges (~0.17 nm).[52] For example, Sushko and Shluger described DNA/mica interactions using a DLVO model for an interaction between a cylinder and a flat surface.[53] It is reasonable to use the sphere-cylinder DLVO model to describe the NP−DNA interaction.

In this study, we determined the binding affinity of selected NPs [positively and negatively charged quantum dots, gold NPs capped with different surface groups (carrying different surface charge), latex beads, as well as silicon, silver, hematite, CeO_2, ZnO, TiO_2 and SiO_2 NPs] for DNA on the basis of the DLVO model. The binding affinity of NPs to DNA was experimentally evaluated with AFM and then compared with the model prediction. Furthermore, the effect of NPs on DNA replication was investigated using the polymerase chain reaction (PCR) technique and then related to the binding affinity of NPs for DNA. The overall goal of this study is to predict the affinity of NPs for DNA and to provide insights into the prediction of the genotoxicity of NPs.

RESULTS AND DISCUSSION

Determination of Parameters in the DLVO Model. The interaction energy between each NP and DNA was computed based on DLVO models for the sphere-cylinder geometry.[54] A number of parameters are required by the model including the size and the surface potential of both NPs and DNA molecules, and the Hamaker constant for NP−DNA interactions.

The sizes of those NPs were measured using AFM (shown in Figure S1 in the Supporting Information) by examining at least 100 randomly picked particles. Statistically, the radii of QDs (+), QDs (−), gold NPs (citrate), gold NPs (COOH), silver NPs, hematite NPs, CeO_2 NPs, ZnO NPs, TiO_2 NPs, SiO_2 NPs, silicon NPs, and latex beads are 8.54 ± 2.46, 7.80 ± 2.05, 2.76 ± 0.54, 13.09 ± 4.60, 6.41 ± 3.19, 8.14 ± 1.44, 42.12 ± 15.20, 45.97 ± 17.22, 12.72 ± 3.09, 13.20 ± 4.13, 15.36 ± 4.50, and 15.15 ± 5.54 nm, respectively.

The surface potential (Ψ_o) of DNA was determined from the Grahame equation,[55] which, under assumption of low potentials below 25 mV, simplifies to

$$\psi_o = \frac{\sigma}{\varepsilon\varepsilon_0\kappa} \quad (1)$$

where σ represents the charge density; ε_0 is the vacuum permittivity; ε is the relative permittivity of water; κ represents the inverse Debye length in the buffer solution, which is calculated to be 0.05 $Å^{-1}$ according to the equation below:

$$\kappa = \sqrt{\frac{\sum_i \rho_{\infty i} e^2 z_i^2}{\varepsilon\varepsilon_0 k_B T}} \quad (2)$$

where k_B is the Boltzmann constant; T is absolute temperature; z_i is the valency of the ith ion; e is unit

charge; and $\rho_{\infty i}$ is the number concentration of the ith ion.

For double-stranded DNA molecules, a value of -0.15 C·m^{-2} was obtained for σ.[56] Thus, ψ_o for DNA was calculated to be -21.5 mV, which agrees well with a previous study.[57]

The surface potentials of NPs were determined from measured electrophoretic mobility (EPM) values *via* the Henry equation:[58]

$$\psi_o = \frac{\mu\eta}{\varepsilon f(\kappa a)} \quad (3)$$

where μ is EPM; ε is the relative permittivity of water; η is the solution viscosity; and $f(\kappa a)$ is Henry's function, which is reasonably well approximated by[58]

$$f(\kappa a) = \frac{2}{3}\left[1 + \frac{1}{2(1+2.5/\kappa a)^3}\right] \quad (4)$$

where κ is still the inverse Debye length and a is the particle radius.[59,60] From eqs 3 and 4, the average surface potentials of QDs (+), QDs (−), gold NPs (citrate), gold NPs (COOH), silver NPs, hematite NPs, CeO_2 NPs, ZnO NPs, TiO_2 NPs, SiO_2 NPs, silicon NPs, and latex beads were determined to be 4.45 ± 1.90, −40.90 ± 2.85, −29.10 ± 0.60, −63.14 ± 2.83, −21.50 ± 0.75, −13.32 ± 1.15, −9.52 ± 1.52, −10.15 ± 0.86, −12.33 ± 0.99, −17.09 ± 0.40, −28.70 ± 1.31, and −33.85 ± 3.00 mV, respectively.

The Hamaker constant (A_H) for the interaction of NPs and DNA in water was determined with Lifshitz theory. For two media of dielectric constants or permittivity ε_1 and ε_2 interacting in a third medium with dielectric constant ε_3, the Hamaker constant is given by[61]

$$A_H \approx \frac{3}{4}kT\left(\frac{\varepsilon_1 - \varepsilon_3}{\varepsilon_1 + \varepsilon_3}\right)\left(\frac{\varepsilon_2 - \varepsilon_3}{\varepsilon_2 + \varepsilon_3}\right) + \frac{3h}{4\pi}\int_{\nu_1}^{\infty}\left(\frac{\varepsilon_1(i\nu) - \varepsilon_3(i\nu)}{\varepsilon_1(i\nu) + \varepsilon_3(i\nu)}\right)\left(\frac{\varepsilon_2(i\nu) - \varepsilon_3(i\nu)}{\varepsilon_2(i\nu) + \varepsilon_3(i\nu)}\right)d\nu \quad (5)$$

where $\varepsilon(i\nu)$ are the values of ε at imaginary frequencies, and $\nu_1 = 2kT\pi/h = 3.9 \times 10^{13}$ s^{-1} at 298 K. The first term in the equation represents the zero-frequency energy of the vdW interaction and includes the Keesom and Debye contributions. The second integration term represents the dispersion energy, *i.e.*, the London contribution. The dielectric constant $\varepsilon(i\nu)$ for nonmetallic particles is expressed by

$$\varepsilon(i\nu) = 1 + (n^2 - 1)/(1 + \nu^2/\nu_0^2) \quad (6)$$

where n represents the refractive index of the medium; ν_0 is the main absorption frequency of the medium. The n values for the DNA molecule, water, hematite, CeO_2 NPs, ZnO NPs, TiO_2 NPs, SiO_2 NPs, silicon NPs, and latex beads are 1.6, 1.33, 3, 2.276, 2.004, 2.488 (anatase), 1.54, 3.5, and 1.59, respectively.[62−64] The ν_0 values for DNA molecule and water are 1.15×10^{15} and 3.0×10^{15} s^{-1}, respectively.[61] The QDs, hematite, CeO_2 NPs, ZnO NPs, TiO_2 NPs, SiO_2 NPs, silicon NPs, and latex beads used in this study, respectively, have maximum absorptions at 530, 190, 310, 190, 260, 230, 470, and 200 nm, corresponding to ν_0 values of 5.66×10^{14}, 1.58×10^{15}, 9.68×10^{14}, 1.58×10^{15}, 1.15×10^{15}, 1.30×10^{15}, 6.38×10^{14}, and 1.50×10^{15} s^{-1}, respectively. The dielectric constant $\varepsilon(i\nu)$ for metallic particles is expressed by

$$\varepsilon(i\nu) = 1 + \nu_e^2/\nu^2 \quad (7)$$

where $\nu_e^2 = n_e e^2/4\pi^2 m_e \varepsilon_0$ is the squared plasma frequency of a free electron gas of number density n_e where m_e is the electron mass. The number densities of gold and silver are 5.90×10^{28} and 5.86×10^{28} m^{-3}, respectively, giving plasma frequencies of $\nu_e = 2.18 \times 10^{15}$ and 2.17×10^{15} s^{-1}, respectively.

The ε values for the DNA molecule, water, hematite, CeO_2 NPs, ZnO NPs, TiO_2 NPs, SiO_2 NPs, silicon NPs, and latex beads are 2.56, 80, 12, 24.3, 8.34, 114, 3.9, 11.68, and 2.52, respectively.[65−68] The ε values for gold and silver are infinity. For CdSe/ZnS QDs, we take an average of the values of ZnS and CdSe, as to our knowledge no calculation method is available to obtain the n and ε values for nanoheterostructures. The dielectric constants for CdSe and ZnS are 9.75 and 8.9, respectively. The refractive indices for CdSe and ZnS are 2.5 and 2.368, respectively.[69] By taking an average, the dielectric constant and refractive index for CdSe/ZnS were, respectively, 9.325 and 2.434. By doing numerical integration in Matlab, the Hamaker constants A_H for DNA interacting with QDs, gold NPs, silver NPs, hematite NPs, CeO_2 NPs, ZnO NPs, TiO_2 NPs, SiO_2 NPs, silicon NPs, and latex beads in liquid were calculated to be 4.0, 3.2, 3.2, 3.9, 2.6, 1.6, 1.7, 2.0, 3.6, and 1.8 kT. The Hamaker constant of each type of NPs as well the particle size and surface potential were listed in Table S1 in the Supporting Information.

Binding Affinity of NPs for DNA. The energy barriers between NPs and DNA, as calculated from the DLVO model, are 0.39 kT for gold (COOH)−DNA, 0.31 kT for latex beads−DNA, 0.18 kT for QDs (−)−DNA, 0.16 kT for silicon−DNA, 0.10 kT for SiO_2−DNA, 0.08 kT for silver−DNA, 0.06 kT for gold (citrate)−DNA, 0.05 kT for TiO_2−DNA, 0.04 kT for ZnO−DNA, 0.02 kT for hematite−DNA, 0.003 kT for CeO_2−DNA, and 0 kT for QDs (+)−DNA (Figure 1). These theoretical calculation results suggest that gold NPs (COOH), latex beads, QDs (−), silicon NPs, and SiO_2 NPs are more likely not to bind to DNA compared with the other NPs, owing to the high energy barrier between these NPs and DNA.

AFM was used to verify the predicted binding affinity of NPs for DNA. DNA molecules looked curved and bent, while the NPs binding to the DNA appeared as large or small dark dots. A DNA image in the absence of NPs was presented in Figure S2 in the Supporting Information. The AFM results showed that NPs have quite different binding affinities for DNA. On one hand, as shown in Figure 2, the QDs (+), silver NPs, hematite

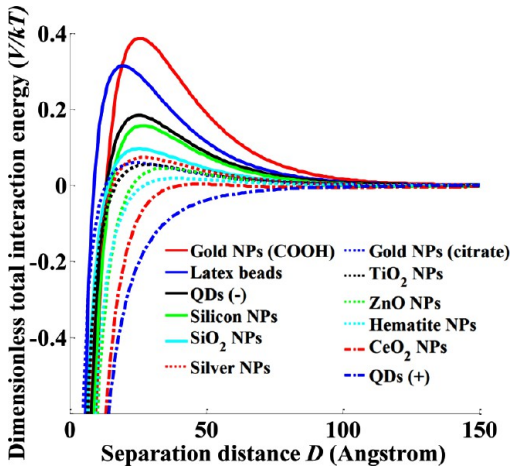

Figure 1. The interaction energy profiles between each NP and DNA.

NPs, gold NPs (citrate), CeO_2 NPs, ZnO NPs and TiO_2 NPs were observed to bind to DNA, which is consistent with our theoretical analysis. On the other hand, the SiO_2 NPs, silicon NPs, QDs (−), gold NPs (COOH) and latex beads did not bind to DNA molecules, which also agreed well with model predictions. It is worth noting that the majority of NPs tested here for DNA interaction were "real" nanosized particles, and therefore our models were applicable in the nanoscale.

We noticed from the AFM image that some NPs appeared to induce DNA bending. The subsequent binding activity of NPs to those bent DNA may not be well described by the sphere−cylinder interaction models proposed in the previous section. Instead, we used a section of torus to represent the bent DNA, and computed the interaction energy between NPs and bent DNA using the sphere-torus model. We found that the relative magnitude of the energy barrier between the bent DNA and each NP was the same as that between the straight DNA and each NP, *i.e.*, the energy barrier height increased in the order of QDs (+) < CeO_2 NPs < hematite NPs < ZnO NPs < TiO_2 NPs < gold NPs (citrate) < silver NPs < SiO_2 NPs < silicon NPs < QDs (−) < latex beads < gold NPs (COOH) under both scenarios.

NPs with a high affinity for DNA may interfere with normal DNA functions. The AFM images in Figure 2 show that the binding of NPs to DNA has the potential to dramatically change the DNA conformation. We can clearly observe the DNA bending or looping in the presence of QDs (+) and hematite NPs. In addition, when silver and ZnO NPs were present, DNA formed a more compact conformation compared to the native random coil conformation. Two additional AFM images were presented in Figure S3 in the Supporting Information for illustrating the compact DNA conformation induced by silver NPs and QDs (+). These observations were discussed in more details in our previous work.[11]

Proteins that are requisite for DNA replication, transcription and repair processes may not function correctly owing to (1) preoccupation of DNA by NPs in the binding sites of proteins (*e.g.*, DNA polymerase/RNA polymerase and sigma factor); (2) conformational changes in DNA resulting in inhibitory structures that block unwinding of DNA or traversing along DNA. In contrast, DNA molecules incubated with SiO_2 NPs, silicon NPs, QDs (−), gold NPs (COOH) and latex beads did not show conformational changes; it is likely that these DNA molecules still allow for normal functions.

We performed the interaction energy calculation between protein and DNA using T7 RNAP as a model protein. Its surface potential was determined as −9.60 ± 2.80 mV according to eq 3. The Hamaker constant (A_H) for protein and DNA interacting in liquid was estimated to be 3 kT.[70] Assuming RNAP has a spherical shape, its radius (nm) was approximated as 3 nm on the basis of its mass M (in daltons) by the relation $R_S = 0.066M^{1/3}$.[71] The result showed that the energy barrier between protein and DNA is 0.01 kT; the binding affinities of QDs (+), silver, hematite, gold (citrate), CeO_2, ZnO and TiO_2 NPs for DNA are of similar magnitude and may compete for binding to DNA molecules with protein.

Effects of NPs on DNA Replication. The PCR method was employed to probe the effect of NPs on DNA replication. The agarose gel electrophoresis results (Figure 3) showed how the 12 types of NPs over a range of concentrations affected DNA replication. The quantity of PCR amplified DNA products was reflected by the intensity of each band. QDs (+) completely inhibited DNA replication at the concentration of 0.15 nM, agreeing with a previous study which showed that cationic QDs caused genotoxic effects.[72] The DNA replication was completely inhibited by silver NPs at 0.05 nM. This is consistent with previous studies which showed silver NPs were genotoxic.[24,73,74] Hematite NPs showed a complete inhibition at 0.2 nM; hematite NPs also have been found to induce genotoxicity.[29,75] Gold NPs (citrate) affected DNA replication at 0.3 nM and completely impeded the replication process at the concentration of 0.5 nM. This agreed with a previous study showing that gold NPs associated with DNA and subsequently induced DNA bending and strand separation.[35] CeO_2 NPs significantly inhibited DNA replication at 0.05 nM. ZnO suppressed the DNA replication process at 0.2 nM. The latex beads also resulted in the inhibition of DNA replication at a high concentration of 1.5 nM. In contrast, other NPs did not show any signs of inhibition at their highest concentration employed in this study (1.4−1.6 nM). The most interesting result comes from TiO_2 NPs. In the binding affinity experiment, we have observed many TiO_2 NPs binding on DNA (Figure 2g); thus, we expected that TiO_2 NPs were likely inhibitory to DNA replication. These seemingly contradictory results could be explained by the enhanced thermal conductivity in the PCR. TiO_2 NPs can induce a rapid increase in thermal

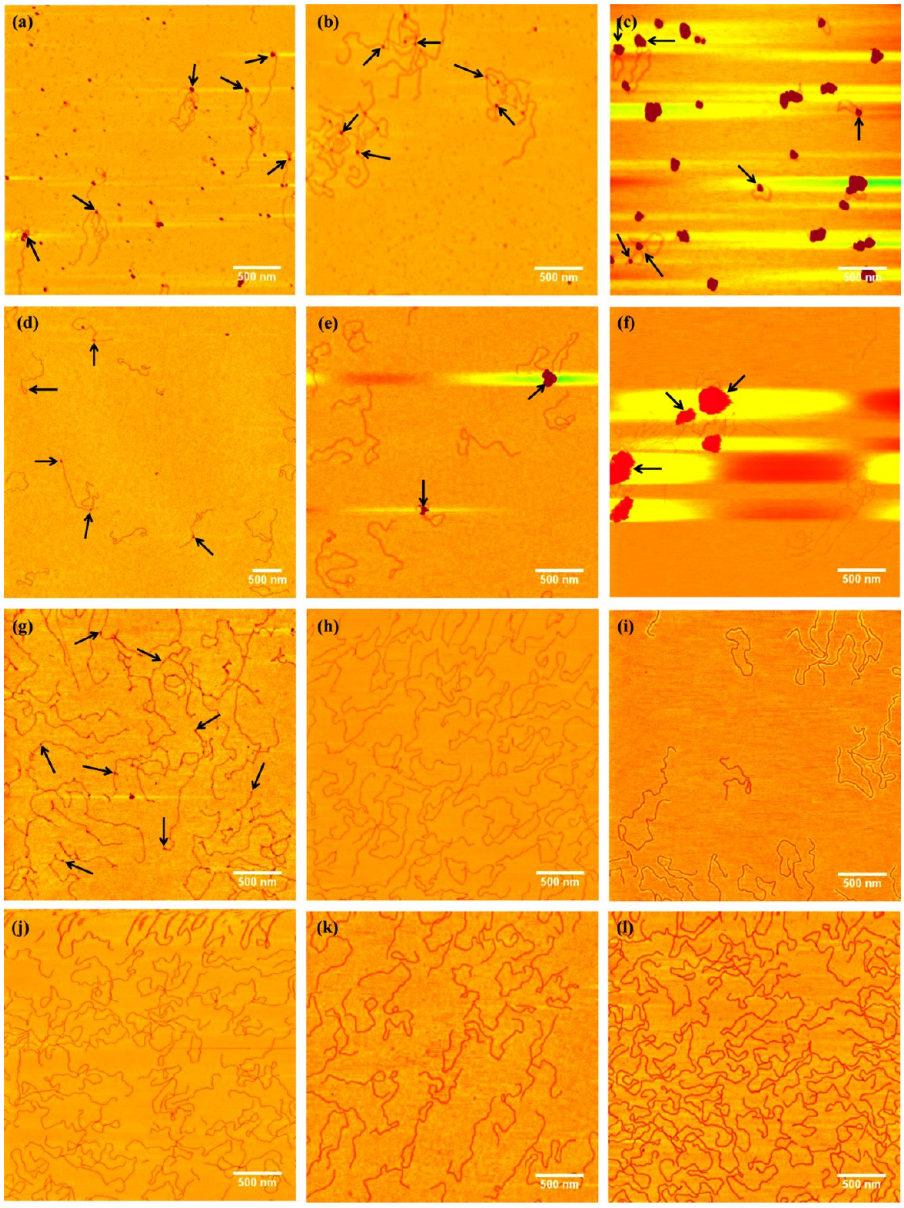

Figure 2. AFM topographical images of DNA molecules after exposure to NPs. DNA molecules were observed under AFM after exposure to (a) QDs (+), (b) silver NPs, (c) hematite NPs, (d) gold NPs (citrate), (e) CeO_2 NPs, (f) ZnO NPs, (g) TiO_2 NPs, (h) SiO_2 NPs, (i) silicon NPs, (j) QDs (−), (k) gold NPs (COOH), and (l) latex beads. The dark dots in (a)−(g), as indicated by black arrows, are NPs, namely, the black arrows indicate representative binding sites of NPs on DNA molecules. SiO_2 NPs, silicon NPs, QDs (−), gold NPs (COOH) and latex beads did not bind to DNA molecules, as observed from (h)−(l).

conductivity sufficient to enhance PCR efficiency,[76] which might offset their inhibitive effects on DNA replication.

We further investigated the relation between the ability of NPs to inhibit DNA replication and the predicted binding affinity of NPs for DNA. As observed from Figure 4, NPs that were predicted to have a high binding affinity (*i.e.*, low energy barrier) for DNA molecules also had a high potential to inhibit DNA replication. This implied that (1) the binding of NPs to DNA is likely an important mechanism for causing the genotoxicity of NPs, and (2) the DLVO model may act as a simple and effective tool for predicting the genotoxicity of NPs induced by the direct binding activity of NPs with DNA. It is noted that the Ag NPs have a higher inhibition ability compared with the model prediction; this is reasonable, as Ag NPs released Ag ions, which may be also detrimental to the DNA replication.[24,77−79]

As mentioned earlier in this paper, oxidative stress resulted from reactive oxygen species (ROS) has been reported as an important cause of genotoxicity of NPs.[80] Our group has conducted a series of studies on the ROS production by NPs.[79,81] However, ROS do not appear to explain the effects of NPs observed here. It is well-known that among the three primary ROS radicals (*i.e.*, ·OH, $^1O_2$, and $O_2^{\bullet-}$), ·OH and $^1O_2$ are mainly responsible for DNA damage.[82,83] Our previous work showed that the ability of NPs to produce ·OH

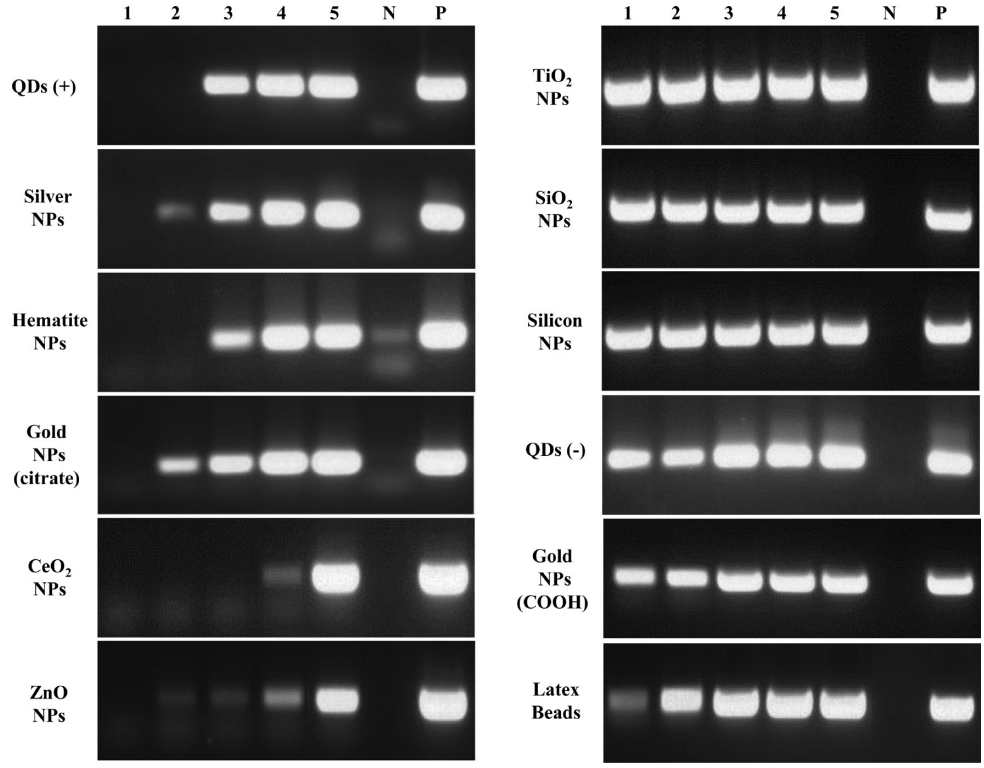

Figure 3. Effects of NPs on DNA replication *in vitro* by quantification of PCR products. A total of 50 ng of linearized pGEMEX-1 was used in each reaction to amplify a 180 bp PCR fragment except for negative control. Each type of NPs was tested under a range of concentrations. From lane 1 to 5, the final concentrations of QDs (+) were 0.2, 0.15, 0.1, 0.05, 0.01 nM, silver NPs were 0.05, 0.03, 0.02, 0.01, 0.002 nM, hematite NPs were 0.5, 0.2, 0.1, 0.05, 0.01 nM, gold NPs (citrate) were 0.5, 0.3, 0.2, 0.1, 0.05 nM, CeO_2 NPs were 0.5, 0.2, 0.1, 0.05, 0.01 nM, ZnO NPs were 2, 0.5, 0.3, 0.2, 0.05 nM, TiO_2, SiO_2 and silicon NPs were all 1.5, 1.0, 0.5, 0.3, 0.2 nM, QDs (−) were 1.6, 0.8, 0.16, 0.08, 0.016 nM, gold NPs (COOH) were 1.4, 1.0, 0.5, 0.3, 0.2 nM, and latex beads were 1.5, 1.0, 0.5, 0.3, 0.2 nM. N and P, respectively, represent the negative and positive controls for the PCR experiment. N: negative control without DNA template and NPs. P: positive control using 50 ng of DNA template without NPs.

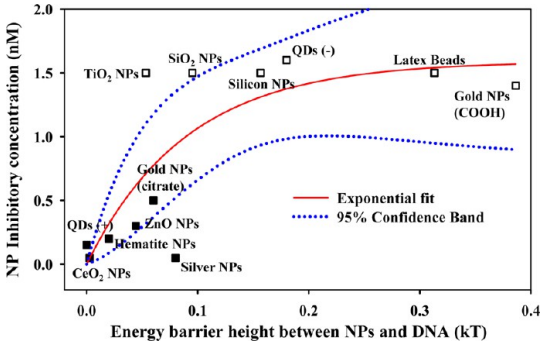

Figure 4. Relationship between the tested concentration of NPs significantly inhibiting DNA replication *in vitro* and the determined energy barrier between NPs and DNA. A significant inhibition occurs when the intensity of the gel electrophoresis band in Figure 3 is below 30% of that of the positive control. TiO_2 NPs, SiO_2 NPs, silicon NPs, QDs (−), gold NPs (COOH) and latex beads (open square) did not show a significant inhibition of DNA replication even at the highest concentration employed in this study, still those NPs were included in the figure for comparison with other NPs that have strong inhibition on DNA replication. Data points represent individual replicates. An exponential regression [$y = 1.59(1 - \exp(-11.10x))$, $r^2 = 0.62$] was performed.

and $^1O_2$ increased in the order of QDs (+)/QDs (−)/CeO_2 NPs < hematite NPs < silver NPs < SiO_2 NPs < ZnO NPs < gold NPs (citrate) < silicon NPs < TiO_2 NPs.[79,81,84] Apparently, the ROS production does not explain the PCR results, because the genotoxicity of NPs was shown to increase in the order of QDs (−)/TiO_2/SiO_2/silicon NPs < gold NPs (citrate) < ZnO NPs < hematite NPs < QDs (+) < CeO_2/silver NPs. Therefore, we may rule out ROS as the primary cause of genotoxicity of NPs in this study; rather, the direct binding activity of NPs to DNA is likely one reasonable genotoxicity mechanism. Overall, the methodology in this study can help researchers screen NPs and prioritize their genotoxicological testing.

Two-Dimensional Diagrams To Determine the Energy Barrier between NPs and DNA. We constructed two-dimensional diagrams (shown in Figure 5) to help researchers determine the interaction energy barrier between a certain type of NPs and DNA. Each diagram was produced under a certain NP Hamaker constant (*e.g.*, 1, 3, 4, and 10 kT). Contour lines were also plotted in the diagram to clearly indicate the height of the energy barrier. As the surface potential of the particle shifts from negative to positive or as the Hamaker constant increases, the energy barrier decreased, indicating that NPs with positive surface potential or a high Hamaker constant have a high affinity for DNA molecules. This is

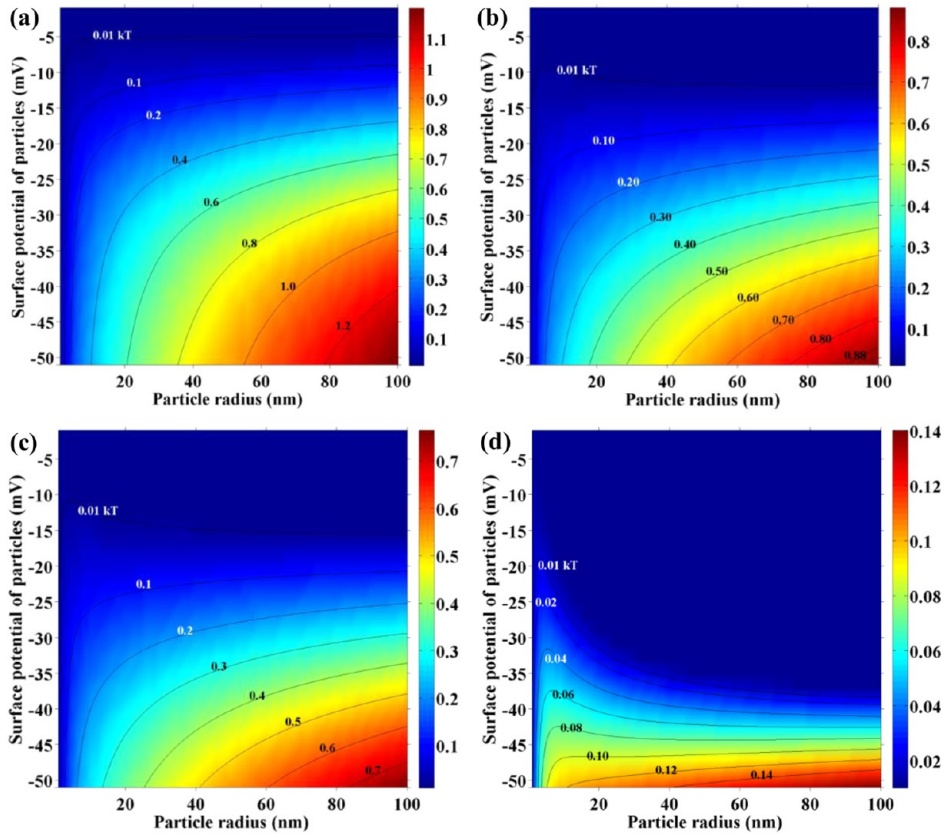

Figure 5. Representative two-dimensional diagrams characterizing the effect of NP size and surface potential on the height of the energy barrier between the particle and DNA. The Hamaker constants of the particles in (a)−(d) are 1, 3, 4, and 10 kT, respectively. The lines are contour lines representing the height of the energy barrier (in units of kT) between the particle and DNA. The color indicates the height of the energy barrier of each pixel.

consistent with a previous study.[70] However, the increase in particle size does not always result in an increase in the height of the energy barrier, which can be observed most obviously in the scenario in which the Hamaker constant of the NPs is 10 kT (Figure 4d). Provided the size, surface potential, and Hamaker constant of a certain type of NPs are known, we can determine the height of the energy barrier between the NPs and DNA molecules, and subsequently estimate the affinity of the NPs for DNA and further evaluate the potential genotoxicity of NPs.

The statement of particle size effect on the energy barrier, *i.e.*, increased particle size does not always result in increased energy barrier, may be less intuitive, but it can be validated by comparing two tested NPs: ZnO and TiO_2 NPs. Their Hamaker constants (1.6 *versus* 1.7 kT) and surface potentials (−10.15 *versus* −12.33 mV) are both quite close, but the particle size of ZnO is much larger than that of TiO_2 NPs. The modeling results showed that ZnO NPs has slightly lower energy barrier with DNA than TiO_2 does (Figure 1). The AFM results showed that ZnO as well as TiO_2 NPs were able to bind to DNA (Figure 2). This example validated the less intuitive size effect of NPs on their interaction energy with DNA.

It is worth noting that the ionic strength of the solution system used in this study is 0.4 M. If different solvent systems with different ionic strength were used, the computed interaction energy results would vary. First, a different ionic strength would alter the Debye length in the solution and subsequently change the surface potential of NPs and DNA. This was addressed by eqs 1−4. In addition, particle size may also be altered due to particle aggregation under a high ionic strength. The aggregation kinetics modeling of NPs has been intensively investigated in our group.[44,85,86] However, we did not incorporate the aggregation model into the theory in the present study, as particle size that we used as the model input was measured after the aggregation has reached slow-aggregation stage, namely, the particle size was pseudostable. Provided that we determine the physicochemical properties (such as the size and surface potential) of NPs under pseudostable states in a new solution, we can still apply the theoretical approach proposed in this study to the new system.

Biological systems are far more complex than the *in vitro* system used in the current study. However, for simplicity, the PCR experiments here employed "naked" DNA (histone-free DNA) similar to that which is present in bacterial cells. This may be a less accurate depiction of human DNA, which is complexed with histones, forming nucleosomes, and further packaged

into chromosomes. However, the nucleosome is not static and has been reported in dynamic equilibrium between wrapped and unwrapped state.[87−89] Nucleosomes spontaneously undergo a conformational fluctuation process called "DNA site exposure", in which a stretch of DNA transiently unwraps off the histone core.[87] The NPs could gain access to DNA sites in such exposed states. We may reasonably infer that NPs that have a high affinity for naked DNA should also have a high affinity for the nucleosome. The experimental validation of this inference using AFM is very challenging, as the size of a chromosome is much larger than that of NPs (μm *versus* nm) and the chromosome has an irregular surface, which would likely makes it more challenging to locate NPs that bind with a chromosome.

Finally, NPs in contact with biological fluids interact with proteins and form a dynamic protein corona, whose composition varies over time and finally reaches equilibrium.[90,91] The existence of the protein corona would reshape the nature of NPs such as the surface potential and particle size. Understanding the protein corona is crucial in predicting nanotoxicity in biological systems.[92] The theoretical methodology in the present study could also be applied to the interaction of NP-protein corona complex with DNA, provided that we know the surface potential, size and composition of the complex in equilibrium. The protein corona may introduce additional non-DLVO forces (especially the hydrogen bonding-induced specific interaction force) into the interaction of NPs with DNA, which under additivity assumption[93] can be incorporated into the theoretical interaction model for describing the interaction between NP-protein corona complexes and DNA.[94] Currently, such studies as well as those using AFM as a tool to probe these interactions are under way in our group.

CONCLUSIONS

In conclusion, this study showed that NPs with a high binding affinity for DNA molecules also have a strong inhibitory effect on DNA replication, while NPs with a low binding affinity for DNA do not. The binding affinity can be predicted by calculating the interaction energy between NPs and DNA on the basis of DLVO models. NPs located in the blue-colored region of the two-dimensional diagrams (Figure 5) are more likely to result in genotoxicity compared with those in the red-colored region. In the future genotoxicological testing of NPs, researchers may be able to prioritize NPs in the blue-colored region, which are predicted to have a high binding affinity for DNA. Also, this study has applications for the rational design of functionalized NPs in DNA labeling, biological imaging and sensing, and drug delivery for medical and therapeutic applications. Finally, although we demonstrate here the effects of direct binding of NPs to DNA, this likely is one of many mechanisms by which NPs can induce genotoxicity in living cells. Additional work is required for a comprehensive understanding of the underlying toxicity mechanisms of NPs and to build an "ultimate" nanotoxicity predictive model that takes into account multiple toxicity mechanisms and their interactions.

MATERIALS AND METHODS

Materials. Two types of water-soluble CdSe/ZnS core/shell quantum dots (QDs), respectively coated with polydiallydimethylammonium chloride (PDDA) and poly(ethylene glycol) (PEG) with a carboxylic acid terminal end group, were purchased from Ocean NanoTech, LLC (Springdale, AR). For convenience, we named the former "QDs (+)" and the latter "QDs (−)", as the electrophoresis experiments showed the former carried positive surface charge while the latter carried negative charge. Citrate-stabilized gold NPs were purchased from Sigma-Aldrich (St. Louis, MO). Gold NPs functionalized with COOH surface group were purchase from Ocean NanoTech, LLC (Springdale, AR). Also for convenience, we named the former "gold NPs (citrate)" and latter "gold NPs (COOH)". Citrate-stabilized silver NPs were purchased from Ted Pella, Inc. (Redding, CA). CeO_2 NPs were purchased from Alfa Aesar (Ward Hill, MA). TiO_2, SiO_2, ZnO NPs and latex beads (30 nm) were purchased from Sigma-Aldrich (St. Louis, MO). Silicon NPs were purchased from the US Research Nanomaterials, Inc. (Houston, TX). Finally, hematite NPs were synthesized in our laboratory using the method of Penners and Koopal[95] with minor modifications.[96] Briefly, 20 mM $FeCl_3$ in 4 mM HCl was incubated at 120 °C in a flask coupled with a water-cooled condenser. The size of the hematite NPs was controlled by incubation time. Approximately 20 min was required to produce hematite NPs of size *ca.* 20 nm.

The sizes and morphologies of those NPs were characterized using AFM (shown in Figure S1 in the Supporting Information). The other characterizations using transmission electron microscopy, dynamic light scattering, X-ray diffraction and/or Fourier transform infrared spectroscopy were published in our previous work.[79,81,84,96,97]

A SacI-linearized plasmid DNA pGEMEX-1 of 3993 base pairs was purchased from Promega Corporation (Madison, WI). The DNA was diluted to 2 nM with sterile TE buffer (10 mM Tris HCl, pH 7.4, 1 mM EDTA) (Fisher Scientific Co.). Images acquired by AFM showed that the DNA can be stored in a 4 °C refrigerator for two months without loss of structural integrity. Finally, the protein used in this study was T7 RNA polymerase (RNAP) purchased from Promega Corporation (Madison, WI).

Determination of the Electrophoretic Mobility (EPM) of NPs and Protein. The EPM of NPs and protein in the TE buffer containing 4 mM Mg^{2+} was measured using a Malvern Zetasizer Nano ZS instrument. In brief, 1.5 mL of NP or protein suspensions of 10 mg/L in the TE buffer containing 4 mM Mg^{2+} was injected into a clean cuvette, and the instrument was then operated with a scattering angle of 173° from the incident laser beam. The autocorrelation function automatically accumulated at least 10 runs for each sample. At least four parallel measurements were made for each condition.

AFM Imaging of the Binding of NPs to DNA. DNA stock solution was diluted to 0.2 nM with sterile TE buffer containing 5 mM Mg^{2+}. The DNA was mixed with NPs at a molar ratio of 1:5 and incubated at 37 °C for 1 h. Then 2.5 μL of the mixture was deposited on a freshly cleaved mica substrate and incubated for 30 min. The mica surface was thoroughly rinsed with Milli-Q pure water and then blown dry with ultrapure nitrogen gas.[11] AFM images were collected at room temperature using an Agilent 5500 Molecular Imaging AFM in the acoustic alternating current (AAC) mode. Silicon cantilevers (BudgetSensors, Bulgaria) with a force constant of approximately 2−5 N/m were used. AFM images were processed using the Picoview 1.12 software from Agilent Technologies.

Effects of NPs on DNA Replication *in Vitro*. The SacI-linearized plasmid DNA pGEMEX-1 (Promega) was used as template to perform the DNA replication assay. A total of 50 ng of DNA template was used to incubate with serial dilutions of NPs for 5 min on ice. The concentrations of NPs used in PCRs are presented in Figure 3. After the incubation step, PCR amplifications were performed in 25 μL reaction volumes with DNA−NP mix, 1 U Phusion High-Fidelity DNA Polymerase (New England Biolabs, MA), 200 μM each dNTP, and 0.5 μM each primer on a Mastercycler pro (Eppendorf). The primers used in the PCR reaction amplify a 180 base pair fragment. The following are the primer sequences:

EP 1: 5′-GGGGATCCGGTACCAGCACCAC-3′

EP 2: 5′-GGGATGTTCCGGCTGCTGACCGT-3′

PCRs began with a denaturation step at 98 °C for 30 s, and 30 cycles of amplification were performed using the following conditions: 30 s at 98 °C, 30 s at 58 °C, and 30 s at 72 °C. Fifteen microliters of each amplified product was used for electrophoresis using 1% agarose gel that was stained with ethidium bromide for visualization.

Conflict of Interest: The authors declare no competing financial interest.

Supporting Information Available: Particle size, surface potential and Hamaker constants of NPs, and the computed energy barrier between each type of NPs and DNA; representative AFM images of NPs; representative AFM images of DNA in the absence of NPs; compact DNA conformation induced by silver NPs and QDs (+); effects of physicochemical properties of NPs on NP−DNA interaction energy. This material is available free of charge *via* the Internet at http://pubs.acs.org.

Acknowledgment. This study was partially supported by the U.S. Environmental Protection Agency Science to Achieve Results Program Grant RD-83385601 and National Science Foundation Grant CBET-1235166. B. K. Hammer and X. Zhao contributions to this work were supported by funds from the Georgia Institute of Technology.

REFERENCES AND NOTES

1. Hussain, S. M.; Braydich-Stolle, L. K.; Schrand, A. M.; Murdock, R. C.; Yu, K. O.; Mattie, D. M.; Schlager, J. J.; Terrones, M. Toxicity Evaluation for Safe Use of Nanomaterials: Recent Achievements and Technical Challenges. *Adv. Mater. (Weinheim, Ger.)* **2009**, *21*, 1549–1559.
2. Pal, S.; Tak, Y. K.; Song, J. M. Does the Antibacterial Activity of Silver Nanoparticles Depend on the Shape of the Nanoparticle? A Study of the Gram-Negative Bacterium *Escherichia coli*. *Appl. Environ. Microbiol.* **2007**, *73*, 1712–1720.
3. Warheit, D. B. How Meaningful Are the Results of Nanotoxicity Studies in the Absence of Adequate Material Characterization? *Toxicol. Sci.* **2008**, *101*, 183–185.
4. Jiang, J. K.; Oberdorster, G.; Biswas, P. Characterization of Size, Surface Charge, and Agglomeration State of Nanoparticle Dispersions for Toxicological Studies. *J. Nanopart. Res.* **2009**, *11*, 77–89.
5. Dhawan, A.; Sharma, V. Toxicity Assessment of Nanomaterials: Methods and Challenges. *Anal. Bioanal. Chem.* **2010**, *398*, 589–605.
6. Bae, E.; Park, H. J.; Lee, J.; Kim, Y.; Yoon, J.; Park, K.; Choi, K.; Yi, J. Bacterial Cytotoxicity of the Silver Nanoparticle Related to Physicochemical Metrics and Agglomeration Properties. *Environ. Toxicol. Chem.* **2010**, *29*, 2154–2160.
7. Keller, A. A.; Wang, H. T.; Zhou, D. X.; Lenihan, H. S.; Cherr, G.; Cardinale, B. J.; Miller, R.; Ji, Z. X. Stability and Aggregation of Metal Oxide Nanoparticles in Natural Aqueous Matrices. *Environ. Sci. Technol.* **2010**, *44*, 1962–1967.
8. Petosa, A. R.; Jaisi, D. P.; Quevedo, I. R.; Elimelech, M.; Tufenkji, N. Aggregation and Deposition of Engineered Nanomaterials in Aquatic Environments: Role of Physicochemical Interactions. *Environ. Sci. Technol.* **2010**, *44*, 6532–6549.
9. Hotze, E. M.; Phenrat, T.; Lowry, G. V. Nanoparticle Aggregation: Challenges to Understanding Transport and Reactivity in the Environment. *J. Environ. Qual.* **2010**, *39*, 1909–1924.
10. Stone, V.; Nowack, B.; Baun, A.; van den Brink, N.; von der Kammer, F.; Dusinska, M.; Handy, R.; Hankin, S.; Hassellov, M.; Joner, E.; Fernandes, T. F. Nanomaterials for Environmental Studies: Classification, Reference Material Issues, and Strategies for Physico-Chemical Characterisation. *Sci. Total Environ.* **2010**, *408*, 1745–1754.
11. Li, K. G.; Zhang, W.; Chen, Y. S. Quantum Dot Binding to DNA: Single-Molecule Imaging with Atomic Force Microscopy. *Biotechnol. J.* **2013**, *8*, 110–116.
12. Zhang, W.; Hughes, J.; Chen, Y. S. Impacts of Hematite Nanoparticle Exposure on Biomechanical, Adhesive, and Surface Electrical Properties of *Escherichia coli* Cells. *Appl. Environ. Microbiol.* **2012**, *78*, 3905–3915.
13. Zhang, W.; Yao, Y.; Chen, Y. S. Imaging and Quantifying the Morphology and Nanoelectrical Properties of Quantum Dot Nanoparticles Interacting with DNA. *J. Phys. Chem. C* **2011**, *115*, 599–606.
14. Desai, M. P.; Labhasetwar, V.; Amidon, G. L.; Levy, R. J. Gastrointestinal Uptake of Biodegradable Microparticles: Effect of Particle Size. *Pharm. Res.* **1996**, *13*, 1838–1845.
15. Desai, M. P.; Labhasetwar, V.; Walter, E.; Levy, R. J.; Amidon, G. L. The Mechanism of Uptake of Biodegradable Microparticles in Caco-2 Cells Is Size Dependent. *Pharm. Res.* **1997**, *14*, 1568–1573.
16. Gaiser, B. K.; Fernandes, T. F.; Jepson, M.; Lead, J. R.; Tyler, C. R.; Stone, V. Assessing Exposure, Uptake and Toxicity of Silver and Cerium Dioxide Nanoparticles from Contaminated Environments. *Environ. Health* **2009**, *8*, 1–4.
17. Moore, M. N. Do Nanoparticles Present Ecotoxicological Risks for the Health of the Aquatic Environment? *Environ. Int.* **2006**, *32*, 967–976.
18. Navarro, E.; Baun, A.; Behra, R.; Hartmann, N. B.; Filser, J.; Miao, A. J.; Quigg, A.; Santschi, P. H.; Sigg, L. Environmental Behavior and Ecotoxicity of Engineered Nanoparticles to Algae, Plants, and Fungi. *Ecotoxicology* **2008**, *17*, 372–386.
19. Nel, A. E.; Madler, L.; Velegol, D.; Xia, T.; Hoek, E. M. V.; Somasundaran, P.; Klaessig, F.; Castranova, V.; Thompson, M. Understanding Biophysicochemical Interactions at the Nano-Bio Interface. *Nat. Mater.* **2009**, *8*, 543–557.
20. Kumar, A.; Pandey, A. K.; Singh, S. S.; Shanker, R.; Dhawan, A. Engineered ZnO and TiO_2 Nanoparticles Induce Oxidative Stress and DNA Damage Leading to Reduced Viability of *Escherichia coli*. *Free Radical Biol. Med.* **2011**, *51*, 1872–1881.
21. Nel, A.; Xia, T.; Madler, L.; Li, N. Toxic Potential of Materials at the Nanolevel. *Science* **2006**, *311*, 622–627.
22. Sanvicens, N.; Marco, M. P. Multifunctional Nanoparticles—Properties and Prospects for Their Use in Human Medicine. *Trends Biotechnol.* **2008**, *26*, 425–433.
23. Soenen, S. J.; Rivera-Gil, P.; Montenegro, J. M.; Parak, W. J.; De Smedt, S. C.; Braeckmans, K. Cellular Toxicity of Inorganic Nanoparticles: Common Aspects and Guidelines for Improved Nanotoxicity Evaluation. *Nano Today* **2011**, *6*, 446–465.
24. AshaRani, P. V.; Mun, G. L. K.; Hande, M. P.; Valiyaveettil, S. Cytotoxicity and Genotoxicity of Silver Nanoparticles in Human Cells. *ACS Nano* **2009**, *3*, 279–290.
25. Park, E. J.; Park, K. Oxidative Stress and Pro-Inflammatory Responses Induced by Silica Nanoparticles *in Vivo* and *in Vitro*. *Toxicol. Lett.* **2009**, *184*, 18–25.
26. Li, J. J.; Zou, L.; Hartono, D.; Ong, C. N.; Bay, B. H.; Yung, L. Y. L. Gold Nanoparticles Induce Oxidative Damage in Lung Fibroblasts *in Vitro*. *Adv. Mater. (Weinheim, Ger.)* **2008**, *20*, 138–142.
27. Xu, A.; Chai, Y. F.; Nohmi, T.; Hei, T. K. Genotoxic Responses to Titanium Dioxide Nanoparticles and Fullerene in *Gpt* Delta Transgenic MEF Cells. *Part. Fibre Toxicol.* **2009**, *6*, 1–13.
28. Trouiller, B.; Reliene, R.; Westbrook, A.; Solaimani, P.; Schiestl, R. H. Titanium Dioxide Nanoparticles Induce DNA Damage and Genetic Instability *in Vivo* in Mice. *Cancer Res.* **2009**, *69*, 8784–8789.
29. Bhattacharya, K.; Davoren, M.; Boertz, J.; Schins, R. P. F.; Hoffmann, E.; Dopp, E. Titanium Dioxide Nanoparticles Induce Oxidative Stress and DNA-Adduct Formation but

Not DNA-Breakage in Human Lung Cells. *Part. Fibre Toxicol.* **2009**, *6*, 1–11.
30. Sharma, V.; Anderson, D.; Dhawan, A. Zinc Oxide Nanoparticles Induce Oxidative Stress and Genotoxicity in Human Liver Cells (HepG2). *J. Biomed. Nanotechnol.* **2011**, *7*, 98–99.
31. Sharma, V.; Shukla, R. K.; Saxena, N.; Parmar, D.; Das, M.; Dhawan, A. DNA Damaging Potential of Zinc Oxide Nanoparticles in Human Epidermal Cells. *Toxicol. Lett.* **2009**, *185*, 211–218.
32. Karlsson, H. L.; Cronholm, P.; Gustafsson, J.; Moller, L. Copper Oxide Nanoparticles Are Highly Toxic: A Comparison between Metal Oxide Nanoparticles and Carbon Nanotubes. *Chem. Res. Toxicol.* **2008**, *21*, 1726–1732.
33. Auffan, M.; Rose, J.; Orsiere, T.; De Meo, M.; Thill, A.; Zeyons, O.; Proux, O.; Masion, A.; Chaurand, P.; Spalla, O.; Botta, A.; Wiesner, M. R.; Bottero, J. Y. CeO_2 Nanoparticles Induce DNA Damage Towards Human Dermal Fibroblasts *in Vitro*. *Nanotoxicology* **2009**, *3*, 161–171.
34. Yang, H.; Liu, C.; Yang, D. F.; Zhang, H. S.; Xi, Z. G. Comparative Study of Cytotoxicity, Oxidative Stress and Genotoxicity Induced by Four Typical Nanomaterials: The Role of Particle Size, Shape and Composition. *J. Appl. Toxicol.* **2009**, *29*, 69–78.
35. Railsback, J. G.; Singh, A.; Pearce, R. C.; McKnight, T. E.; Collazo, R.; Sitar, Z.; Yingling, Y. G.; Melechko, A. V. Weakly Charged Cationic Nanoparticles Induce DNA Bending and Strand Separation. *Adv. Mater. (Weinheim, Ger.)* **2012**, *24*, 4261–4265.
36. Takenaka, S.; Yamashita, K.; Takagi, M.; Hatta, T.; Tanaka, A.; Tsuge, O. Study of the DNA Interaction with Water-Soluble Cationic Fullerene Derivatives. *Chem. Lett.* **1999**, 319–320.
37. Zhao, X. C.; Striolo, A.; Cummings, P. T. C_{60} Binds to and Deforms Nucleotides. *Biophys. J.* **2005**, *89*, 3856–3862.
38. Han, G.; Chari, N. S.; Verma, A.; Hong, R.; Martin, C. T.; Rotello, V. M. Controlled Recovery of the Transcription of Nanoparticle-Bound DNA by Intracellular Concentrations of Glutathione. *Bioconjugate Chem.* **2005**, *16*, 1356–1359.
39. McIntosh, C. M.; Esposito, E. A.; Boal, A. K.; Simard, J. M.; Martin, C. T.; Rotello, V. M. Inhibition of DNA Transcription Using Cationic Mixed Monolayer Protected Gold Clusters. *J. Am. Chem. Soc.* **2001**, *123*, 7626–7629.
40. You, C. C.; Chompoosor, A.; Rotello, V. M. The Biomacromolecule-Nanoparticle Interface. *Nano Today* **2007**, *2*, 34–43.
41. Johnston, H. J.; Hutchison, G.; Christensen, F. M.; Peters, S.; Hankin, S.; Stone, V. A Review of the *in Vivo* and *in Vitro* Toxicity of Silver and Gold Particulates: Particle Attributes and Biological Mechanisms Responsible for the Observed Toxicity. *Crit. Rev. Toxicol.* **2010**, *40*, 328–346.
42. Turro, C. Binding Manners. *Nat. Chem.* **2012**, *4*, 591.
43. Li, K. G.; Chen, Y.; Zhang, W.; Pu, Z. C.; Jiang, L.; Chen, Y. S. Surface Interactions Affect the Toxicity of Engineered Metal Oxide Nanoparticles toward *Paramecium*. *Chem. Res. Toxicol.* **2012**, *25*, 1675–1681.
44. Li, K. G.; Chen, Y. S. Effect of Natural Organic Matter on the Aggregation Kinetics of CeO_2 Nanoparticles in Kcl and Cacl2 Solutions: Measurements and Modeling. *J. Hazard. Mater.* **2012**, *209*, 264–270.
45. Puzyn, T.; Rasulev, B.; Gajewicz, A.; Hu, X. K.; Dasari, T. P.; Michalkova, A.; Hwang, H. M.; Toropov, A.; Leszczynska, D.; Leszczynski, J. Using Nano-QSAR to Predict the Cytotoxicity of Metal Oxide Nanoparticles. *Nat. Nanotechnol.* **2011**, *6*, 175–178.
46. Cao, Q. Q.; Zuo, C. C.; Ma, Y. H.; Li, L. J.; Zhang, Z. Interaction of Double-Stranded DNA with a Nanosphere: A Coarse-Grained Molecular Dynamics Simulation Study. *Soft Matter* **2011**, *7*, 506–514.
47. Derjaguin, B.; Landau, L. Theory of the Stability of Strongly Charged Lyophobic Sols and of the Adhesion of Strongly Charged Particles in Solutions of Electrolytes. *Acta Physicochim. URSS* **1941**, *14*, 633–662.
48. Verwey, E. J. W.; Overbeek, J. T. G.; Nes, K. V. *Theory of the Stability of Lyophobic Colloids; the Interaction of Sol Particles Having an Electric Double Layer*; Elsevier Pub. Co.: New York, 1948; p xi, 205 p.
49. Schellman, J. A.; Stigter, D. Electrical Double Layer, Zeta Potential, and Electrophoretic Charge of Double-Stranded DNA. *Biopolymers* **1977**, *16*, 1415–1434.
50. Stigter, D. Interactions of Highly Charged Colloidal Cylinders with Applications to Double-Stranded DNA. *Biopolymers* **1977**, *16*, 1435–1448.
51. Sharp, K. A.; Honig, B. Electrostatic Interactions in Macromolecules—Theory and Applications. *Annu. Rev. Biophys. Biophys. Chem.* **1990**, *19*, 301–332.
52. Harries, D. Solving the Poisson-Boltzmann Equation for Two Parallel Cylinders. *Langmuir* **1998**, *14*, 3149–3152.
53. Sushko, M. L.; Shluger, A. L. Dlvo Theory for Like-Charged Polyelectrolyte and Surface Interactions. *Mater. Sci. Eng., C* **2007**, *27*, 1090–1095.
54. Li, K. G.; Chen, Y. S. Evaluation of DLVO Interaction between a Sphere and a Cylinder. *Colloids Surf., A* **2012**, *415*, 218–229.
55. Butt, H.-J.; Graf, K.; Kappl, M. *Physics and Chemistry of Interfaces*, 2nd., rev. and enl. ed.; Wiley-VCH: Weinheim, 2006; p x, 386 p.
56. Hubbard, A. T. *Encyclopedia of Surface and Colloid Science*; Marcel Dekker: New York, 2002; p 4 v. (5667 p).
57. Park, I. K.; Kim, T. H.; Park, Y. H.; Shin, B. A.; Choi, E. S.; Chowdhury, E. H.; Akaike, T.; Cho, C. S. Galactosylated Chitosan-Graft-Poly(Ethylene Glycol) as Hepatocyte-Targeting DNA Carrier. *J. Controlled Release* **2001**, *76*, 349–362.
58. Kirby, B. Micro- and Nanoscale Fluid Mechanics Transport in Microfluidic Devices. Cambridge University Press: New York; p 1 online resource (xxiii, 512 p). http://prx.library.gatech.edu/login?url= http://www.netLibrary.com/urlapi.asp?action=summary&v=1&bookid=335197.
59. Kirby, B. *Micro- and Nanoscale Fluid Bechanics: Transport in Microfluidic Devices*, 1st ed.; Cambridge University Press: New York, 2010; p 513.
60. Ohshima, H. *Theory of Colloid and Interfacial Electric Phenomena*, Academic Press: Amsterdam; London, 2006; p xvi, 473 p.
61. Israelachvili, J. *Intermolecular and Surface Forces*, 2nd ed.; Academic Press: London; San Diego, CA, 1991; p xxi, 450 p.
62. Munoz, O.; Volten, H.; Hovenier, J. W.; Min, M.; Shkuratov, Y. G.; Jalava, J. P.; van der Zande, W. J.; Waters, L. B. F. M. Experimental and Computational Study of Light Scattering by Irregular Particles with Extreme Refractive Indices: Hematite and Rutile. *Astron. Astrophys.* **2006**, *446*, 525–535.
63. Bueno, R. M.; MartinezDuart, J. M.; HernandezVelez, M.; Vazquez, L. Optical and Structural Characterization of r.f. Sputtered CeO_2 Thin Films. *J. Mater. Sci.* **1997**, *32*, 1861–1865.
64. Bass, M.; Optical Society of America. *Handbook of Optics*, 2nd ed.; McGraw-Hill: New York, 1995.
65. Cha, H. G.; Song, J.; Kim, H. S.; Shin, W.; Yoon, K. B.; Kang, Y. S. Facile Preparation of Fe_2O_3 Thin Film with Photoelectrochemical Properties. *Chem. Commun. (Cambridge, U.K.)* **2011**, *47*, 2441–2443.
66. Yamamoto, T.; Momida, H.; Hamada, T.; Uda, T.; Ohno, T. First-Principles Study of Dielectric Properties of Cerium Oxide. *Thin Solid Films* **2005**, *486*, 136–140.
67. Catlow, C. R. A.; French, S. A.; Sokol, A. A.; Al-Sunaidi, A. A.; Woodley, S. M. Zinc Oxide: A Case Study in Contemporary Computational Solid State Chemistry. *J. Comput. Chem.* **2008**, *29*, 2234–2249.
68. Bergstrom, L. Hamaker Constants of Inorganic Materials. *Adv. Colloid Interface Sci.* **1997**, *70*, 125–169.
69. The Semiconductors-Information Website. http://www.semiconductors.co.uk/propiivi5410.htm (access year 2012).
70. Paillusson, F.; Dahirel, V.; Jardat, M.; Victor, J. M.; Barbi, M. Effective Interaction between Charged Nanoparticles and DNA. *Phys. Chem. Chem. Phys.* **2011**, *13*, 12603–12613.
71. Erickson, H. P. Size and Shape of Protein Molecules at the Nanometer Level Determined by Sedimentation, Gel Filtration, and Electron Microscopy. *Biol. Proced. Online* **2009**, *11*, 32–51.
72. Tiwari, D. K.; Jin, T.; Behari, J. Bio-Distribution and Toxicity Assessment of Intravenously Injected Anti-Her2 Antibody

Conjugated CdSe/ZnS Quantum Dots in Wistar Rats. *Int. J. Nanomed.* **2011**, *6*, 463–475.
73. Asare, N.; Instanes, C.; Sandberg, W. J.; Refsnes, M.; Schwarze, P.; Kruszewski, M.; Brunborg, G. Cytotoxic and Genotoxic Effects of Silver Nanoparticles in Testicular Cells. *Toxicology* **2012**, *291*, 65–72.
74. de Lima, R.; Seabra, A. B.; Duran, N. Silver Nanoparticles: A Brief Review of Cytotoxicity and Genotoxicity of Chemically and Biogenically Synthesized Nanoparticles. *J. Appl. Toxicol.* **2012**, *32*, 867–879.
75. Bhattacharya, K.; Hoffmann, E.; Schins, R. F. P.; Boertz, J.; Prantl, E. M.; Alink, G. M.; Byrne, H. J.; Kuhlbusch, T. A. J.; Rahman, Q.; Wiggers, H.; Schulz, C.; Dopp, E. Comparison of Micro- and Nanoscale Fe^{+3}-Containing (Hematite) Particles for Their Toxicological Properties in Human Lung Cells *in Vitro*. *Toxicol. Sci.* **2012**, *126*, 173–182.
76. Khaliq, A.; Sonawane, P. J.; Sasi, B. K.; Sahu, B. S.; Pradeep, T.; Das, S. K.; Mahapatra, N. R. Enhancement in the Efficiency of Polymerase Chain Reaction by TiO_2 Nanoparticles: Crucial Role of Enhanced Thermal Conductivity. *Nanotechnology* **2010**, *21*, 255704–255804.
77. Park, E. J.; Yi, J.; Kim, Y.; Choi, K.; Park, K. Silver Nanoparticles Induce Cytotoxicity by a Trojan-Horse Type Mechanism. *Toxicol. In Vitro* **2010**, *24*, 872–878.
78. Marambio-Jones, C.; Hoek, E. M. V. A Review of the Antibacterial Effects of Silver Nanomaterials and Potential Implications for Human Health and the Environment. *J. Nanopart. Res.* **2010**, *12*, 1531–1551.
79. Zhang, W.; Li, Y.; Niu, J. F.; Chen, Y. S. Photogeneration of Reactive Oxygen Species on Uncoated Silver, Gold, Nickel, and Silicon Nanoparticles and Their Antibacterial Effects. *Langmuir* **2013**, *29*, 4647–4651.
80. Meng, H.; Xia, T.; George, S.; Nel, A. E. A Predictive Toxicological Paradigm for the Safety Assessment of Nanomaterials. *ACS Nano* **2009**, *3*, 1620–1627.
81. Li, Y.; Zhang, W.; Niu, J. F.; Chen, Y. S. Mechanism of Photogenerated Reactive Oxygen Species and Correlation with the Antibacterial Properties of Engineered Metal-Oxide Nanoparticles. *ACS Nano* **2012**, *6*, 5164–5173.
82. Wiseman, H.; Halliwell, B. Damage to DNA by Reactive Oxygen and Nitrogen Species: Role in Inflammatory Disease and Progression to Cancer. *Biochem. J.* **1996**, *313*, 17–29.
83. Cooke, M. S.; Evans, M. D.; Dizdaroglu, M.; Lunec, J. Oxidative DNA Damage: Mechanisms, Mutation, and Disease. *FASEB J.* **2003**, *17*, 1195–1214.
84. Li, Y.; Zhang, W.; Li, K.; Yao, Y.; Niu, J.; Chen, Y. Oxidative Dissolution of Polymer-Coated CdSe/ZnS Quantum Dots under UV Irradiation: Mechanisms and Kinetics. *Environ. Pollut.* **2012**, *164*, 259–266.
85. Li, K.; Zhang, W.; Huang, Y.; Chen, Y. Aggregation Kinetics of CeO_2 Nanoparticles in KCl and $CaCl_2$ Solutions: Measurements and Modeling. *J. Nanopart. Res.* **2011**, *13*, 6483–6491.
86. Zhang, W.; Crittenden, J.; Li, K. G.; Chen, Y. S. Attachment Efficiency of Nanoparticle Aggregation in Aqueous Dispersions: Modeling and Experimental Validation. *Environ. Sci. Technol.* **2012**, *46*, 7054–7062.
87. Li, G.; Levitus, M.; Bustamante, C.; Widom, J. Rapid Spontaneous Accessibility of Nucleosomal DNA. *Nat. Struct. Mol. Biol.* **2005**, *12*, 46–53.
88. Li, G.; Widom, J. Nucleosomes Facilitate Their Own Invasion. *Nat. Struct. Mol. Biol.* **2004**, *11*, 763–769.
89. Polach, K. J.; Widom, J. Mechanism of Protein Access to Specific DNA-Sequences in Chromatin—A Dynamic Equilibrium-Model for Gene-Regulation. *J. Mol. Biol.* **1995**, *254*, 130–149.
90. Cedervall, T.; Lynch, I.; Lindman, S.; Berggard, T.; Thulin, E.; Nilsson, H.; Dawson, K. A.; Linse, S. Understanding the Nanoparticle-Protein Corona Using Methods to Quantify Exchange Rates and Affinities of Proteins for Nanoparticles. *Proc. Natl. Acad. Sci. U.S.A.* **2007**, *104*, 2050–2055.
91. Dell'Orco, D.; Lundqvist, M.; Oslakovic, C.; Cedervall, T.; Linse, S. Modeling the Time Evolution of the Nanoparticle-Protein Corona in a Body Fluid. *PLoS One* **2010**, *5*, e10949.
92. Lesniak, A.; Fenaroli, F.; Monopoli, M. R.; Aberg, C.; Dawson, K. A.; Salvati, A. Effects of the Presence or Absence of a Protein Corona on Silica Nanoparticle Uptake and Impact on Cells. *ACS Nano* **2012**, *6*, 5845–5857.
93. Benos, P. V.; Bulyk, M. L.; Stormo, G. D. Additivity in Protein-DNA Interactions: How Good an Approximation Is It? *Nucleic Acids Res.* **2002**, *30*, 4442–4451.
94. Vonhippel, P. H.; Berg, O. G. On the Specificity of DNA-Protein Interactions. *Proc. Natl. Acad. Sci. U.S.A.* **1986**, *83*, 1608–1612.
95. Penners, N. H. G.; Koopal, L. K. Preparation and Optical Properties of Homodisperse Hematite Hydrosols. *Colloids Surf.* **1986**, *19*, 337–349.
96. Zhang, W.; Rittmann, B.; Chen, Y. S. Size Effects on Adsorption of Hematite Nanoparticles on *E. coli* Cells. *Environ. Sci. Technol.* **2011**, *45*, 2172–2178.
97. Zhang, W.; Yao, Y.; Sullivan, N.; Chen, Y. S. Modeling the Primary Size Effects of Citrate-Coated Silver Nanoparticles on Their Ion Release Kinetics. *Environ. Sci. Technol.* **2011**, *45*, 4422–4428.